Eur. Phys. J. A **27**, 137–141 (2006)
DOI 10.1140/epja/i2005-10196-9

THE EUROPEAN PHYSICAL JOURNAL A

Shape-driving effect of the proton 1/2[541] band in ^{171}Ta

L.H. Zhu[1,a], Z.L. Zhang[1,2], X.G. Wu[1], F.R. Xu[6], G.S. Li[1], Z.M. Wang[1], C.Y. He[1], Y. Wang[1,2], R. Meng[1,2], H.B. Sun[7], R.G. Ma[1], X.Z. Cui[1,2], Y. Liu[1], S.X. Wen[1], Y. Zheng[3], A. Pasternak[4], H.Y. Zhou[5], Y.Z. Liu[2], and C.X. Yang[1,2,5]

[1] China Institute of Atomic Energy, Beijing 102314, PRC
[2] College of Physics, Jilin University, Changchun 130023, PRC
[3] Institute of Modern Physics, Lanzhou 730000, PRC
[4] Cyclotron Lab., A.F. Ioffe Physical Technical Institute, St. Petersburg, Russia
[5] Institute of Low Energy Nuclear Physics, Beijing Normal University, Beijing 100875, PRC
[6] School of Physics, Peking University, Beijing 100871, PRC
[7] School of Science, Shenzhen University, Shenzhen 518060, PRC

Received: 27 January 2005 / Revised version: 10 January 2006 /
Published online: 14 March 2006 –
Communicated by D. Schwalm

Abstract. High-spin states in ^{171}Ta were populated through the heavy-ion fusion-evaporation reaction ^{157}Gd(^{19}F, 5n)^{171}Ta at 105 MeV beam energy. Lifetimes of the levels of the $\pi h_{9/2}1/2[541]$ band have been measured by using the Doppler shift attenuation method. The transition quadrupole moments ($Q_{\rm t}$) and the quadrupole deformation (β_2) have been extracted. Both β_2 and $Q_{\rm t}$ values decrease slightly with increasing rotational frequency. The average β_2 value of 0.26 is 18% larger than that of the $\pi h_{11/2}$ 9/2[514] band. Total Routhian Surface calculations have been performed with the non-axial deformed Woods-Saxon potential and the predicted values of the quadrupole deformation β_2 are in good agreement with that deduced from our lifetime measurement. The shape-driving effect is discussed.

PACS. 21.10.Tg Lifetimes – 23.20.-g Electromagnetic transitions – 27.70.+q $150 \leq A \leq 189$

1 Introduction

The well-known phenomenon of configuration dependence of the neutron AB crossing and the delayed alignment of $i_{13/2}$ neutrons have been frequently observed in the $h_{9/2}$ proton 1/2[541] band of the rare-earth odd-proton nuclei, compared to bands with other configurations and their even-even neighbors [1–10]. The shift of the crossing frequency in the 1/2[541] band has been interpreted as a deformation-driving effect, *i.e.* the high-j low-Ω intruder 1/2[541] proton with a rather large quadrupole orbital moment drives the core to a larger quadrupole deformation, in turn, rising the crossing frequency. However, deformations were often underestimated by the theoretical calculations of the Total Routhian Surface (TRS) or of the Potential Energy Surface (PES) based on the Cranked Shell Model (CSM). The theoretical values of the delayed crossing frequencies in the 1/2[541] bands are usually much smaller than the experimentally observed values [1, 11, 12]. The systematic occurrence of the discrepancy between theoretical calculations and experimental results is a challenge to the present theory. It might indicate that the p-n interaction between the odd proton and the aligned $i_{13/2}$ neutron pair has only been partly and indirectly taken into account in the mean-field theory. In general, the information about quadrupole deformation can be obtained directly from lifetime measurements of energy levels. Therefore, it is important to have experimental measurements of the lifetimes associated with the 1/2[541] band in the band crossing region. Until now, few lifetime measurements for the 1/2[541] band in odd-proton rare-earth nuclei have been made. This paper presents new experimental results on the $h_{9/2}$ proton 1/2[541] band in ^{171}Ta obtained with the Doppler Shift Attenuation Method (DSAM).

2 Experimental method and data analysis

High-spin states in ^{171}Ta were populated through the heavy-ion fusion-evaporation reaction ^{157}Gd(^{19}F, 5n)^{171}Ta at a projectile energy of 105 MeV. The ^{19}F beam was provided by the HI-13 tandem accelerator at the China Institute of Atomic Energy (CIAE). The target consisted of 2.5 mg/cm^2 ^{157}Gd backed with 15.1 mg/cm^2 of natural lead. The ^{157}Gd was isotopically enriched to 97.3%. The thickness of the lead backing

[a] e-mail: zhulh@iris.ciae.ac.cn

was sufficient to slow down and stop the recoils and to allow DSAM lifetime measurements to be performed. The γ-rays emitted from the excited residuals were detected in γ-γ coincidence measurement with a multi-detector array consisting of eleven HPGe detectors, each equipped with a BGO Compton suppression shield in order to enhance photo peaks relative to the Compton background. In the multi-detector array, three detectors were placed at 90°, four at about 48° and four at about 132° with respect to the beam direction. The relative efficiency of the detectors was calibrated using the ^{152}Eu standard source. A total of about 144×10^6 double- or higher-fold coincidence events were recorded in event-by-event mode in the present experiment. The data were sorted off-line into two asymmetric E_γ-E_γ matrices by placing events recorded at specific angles (48° and 132°) on the x-axis, while events recorded at all other angles on the y-axis. The γ-ray lineshapes were obtained using the Radware package [13] by putting gates on the y-axis and projecting the spectra on the x-axis with background subtraction. The Doppler-shift–attenuated lineshapes were observed for the γ-rays above the $I = 29/2\hbar$ level of the 1/2[541] band in ^{171}Ta at both forward and backward angles when summing the gates set on γ-rays below the level of interest. As an example, the lineshapes of the 650 keV γ-ray of ^{171}Ta are shown in fig. 1. The lifetimes of different states were extracted by fitting these experimental lineshapes with an updated version of the DSAM packages composed of the computer codes COMPA, GAMMA and SHAPE [14].

The stopping power, the lineshape response of the detectors, the initial status of the recoil, the sidefeeding pattern and the time evolution of the populated level were carefully considered in our DSAM lifetime analysis.

In the calculation of the stopping power of the recoils, the method described in ref. [14] was adopted. For the electronic stopping power, the Lindhard-Scharf-Schiott (LSS) [15] correction factors were chosen to be $f_e = 1.23$ and 1.13 for Ta recoiling in the Gd target and Pb backing, respectively. For the nuclear stopping power, the calculations based on Ziegler, Biersack and Littmark (ZBL) [16] were adopted. The accuracy of the stopping-power evaluation was estimated to be less than 10%.

The intrinsic lineshape response of the detector was represented by a Gaussian function together with two exponential tails, and was calibrated using radioactive sources.

The most serious limitation for DSAM analysis is the sidefeeding of the levels and the initial status of the recoil. The entry state distributions of residual nuclei were calculated by the Monte Carlo code COMPA based on the statistical model of nuclear reaction, *i.e.* the information about the recoil velocity of residual nucleus, its polar angle with respect to the beam axis, the depth of its creation inside the target as well as the excitation energy and spin of the entry state. Some details of the simulation procedure were described in ref. [14]. The top part of fig. 2 shows the entry state distribution of ^{171}Ta after evaporation of 5 neutrons from the ^{176}Ta compound nucleus calculated

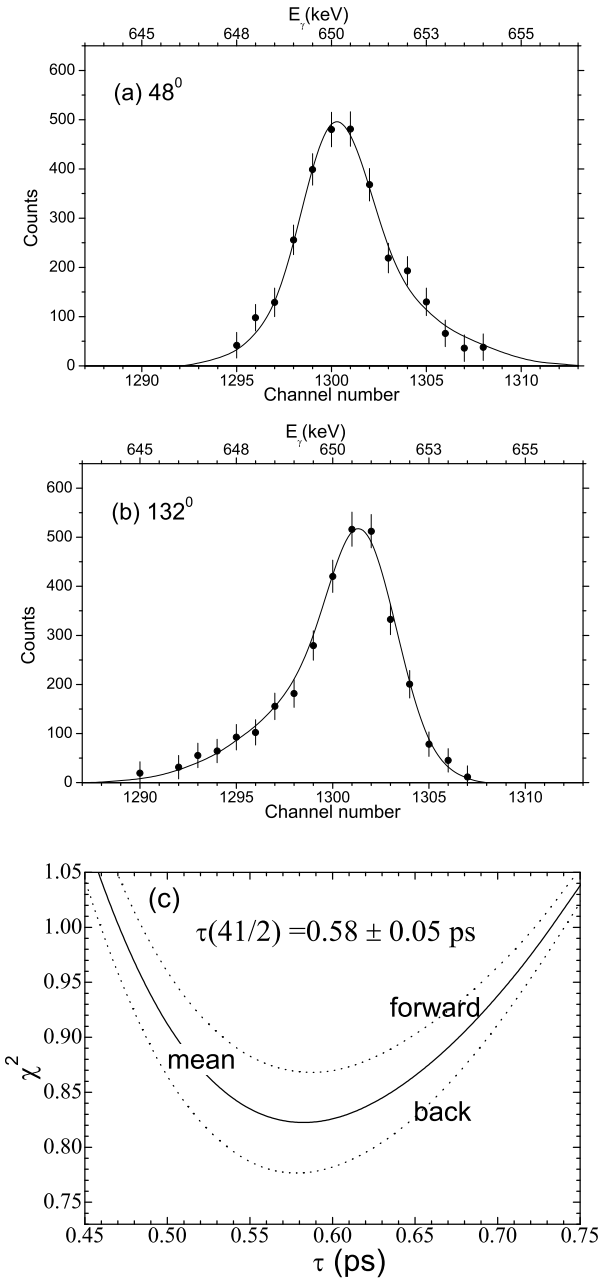

Fig. 1. The Doppler shift lineshapes of the 650 keV $41/2^- \rightarrow 37/2^-$ transition observed in the forward (a, 48°) and backward (b, 132°) angles. The smooth curves represent the simulated lineshapes. (c) The χ^2 *vs.* τ curves from the least-square fit, the dotted lines represent the results of the analysis in the forward and backward angle. The solid line is a mean of these two results.

by the code COMPA. The time distributions of sidefeeding γ-cascades started from the entry state region to two different yrast levels of ^{171}Ta are also shown in fig. 2b.

The sidefeeding pattern and the time evolution of the populated level could not only influence the time distribution of the level population but also the intensity distribution along the band. The parameters in our calculations for all levels are the same and the most important parameters are the quadrupole moments Q_0 of $E2$ stretched

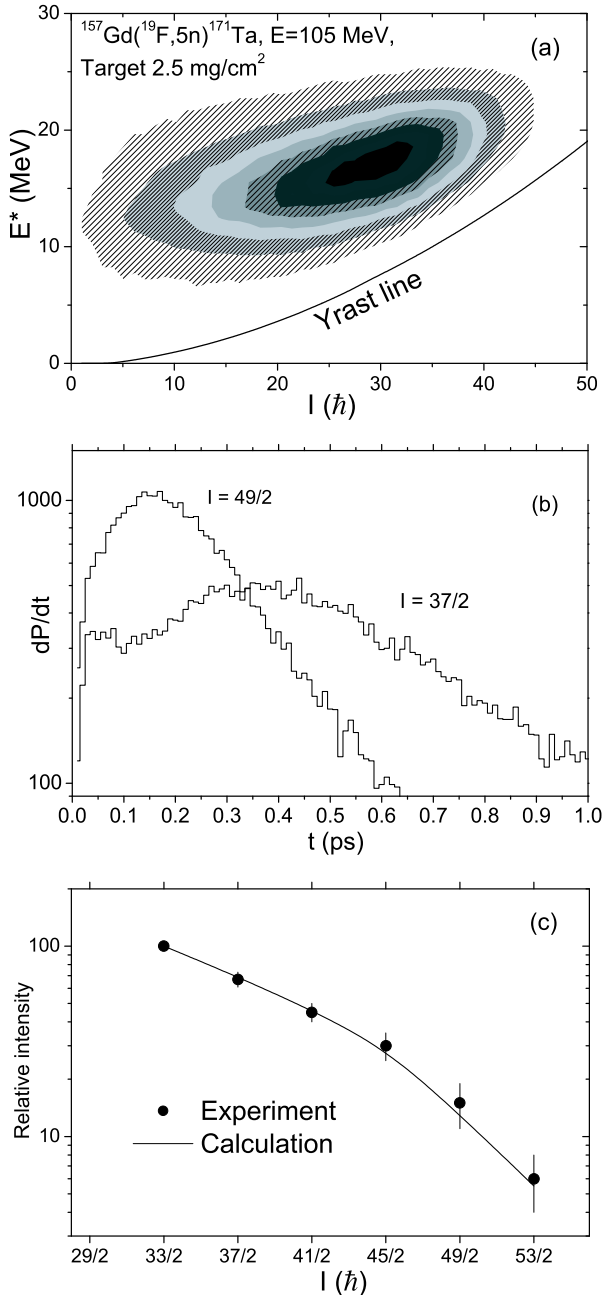

Fig. 2. (a) Distribution of entry states following 5 neutrons evaporated from the compound nucleus ^{176}Ta. (b) Time distribution of sidefeeding γ-cascades starting from the entry states to the 37/2 and 49/2 yrast levels of ^{171}Ta. (c) Experimental and calculated relative intensities along the 1/2[541] band of ^{171}Ta. Calculations have been performed at the same set of parameters, which has been used for the sidefeeding time distributions. 10^6 Monte Carlo events have been simulated.

sidefeeding cascades. In addition, the effects of the fast statistical transitions (mainly $E1$) were taken into account for the high-spin levels close to the entry state. In the calculations, for the $I < 30\hbar$ region, Q_0 has been chosen as $Q_0 = 8$ eb, whereas for the high-spin region Q_0 has been chosen as $Q_0 = 10$ eb. The calculated intensity distribution of the 1/2[541] band was compared with experimental data in fig. 2c, which supports the chosen values of Q_0 with accuracy about ± 2 eb. The systematical errors of the evaluated lifetimes resulted from the uncertainties of Q_0 were estimated to be about 0.05 ps for high-spin levels and 0.1 ps for low-spin levels.

The code GAMMA consecutively extracted each event from the output file of the code COMPA and simulated a number of 10^6 histories of the slowing-down and multiple scattering of the recoils in the stopper material, the cascade γ-transitions from the entry state as well as the γ-absorption in the detectors by means of Monte Carlo techniques. The code GAMMA took into account not only the cascade feeding along the given level scheme but also the sidefeeding cascade from each entry state. Finally, the program SHAPE performed a fit to the γ-ray shape of the gated spectra mentioned above, and the determination of lifetime (τ) based on the χ^2 analysis.

The lifetime analyses of six energy levels from spin 33/2 to 53/2 in the 1/2[541] band of ^{171}Ta were carried out. As a typical example the experimental and simulated lineshapes for the 650 keV transition from the $41/2^-$ level at 48° and 132° are shown in fig. 1. The closed circles represent the experimental values (the error bars indicate the statistical errors after background subtraction) and the solid lines represent the simulated lineshapes. The χ^2 curves from the least-square fit to the 650 keV lineshapes are also given in fig. 1. The dotted lines represent forward and backward results, and the solid line represents the average result. The lifetime of the $41/2^-$ level was determined to be 0.58(7) ps. The uncertainty in lifetime includes the statistical errors and the uncertainties in side- and cascade feedings, as well as those of the stopping powers in target and backing.

3 Results and discussions

A band crossing of the $h_{9/2}$ proton 1/2[541] band in ^{171}Ta had been previously observed [9] at frequency $\hbar\omega = 0.29$ MeV and spin about $I = 33/2\hbar$. Figure 3 shows a partial level scheme of this band around the crossing region and the lifetimes measured in the present work. The transition energies and the relative intensities are shown in the right side and left side of the level scheme, respectively. The lifetimes of six levels from spin 33/2 to $53/2\hbar$ are listed in the right column of fig. 3. For the 608 keV and 699 keV transitions contamination lines have been taken into account in the lineshape analysis. For the lifetime of the $33/2^-$ state, only the lower limit is given due to the small Doppler shift of the 570 keV transition.

A summary of the results for the 1/2[541] band is presented in table 1. The lifetimes, reduced transition probabilities $B(E2)$ and the transition quadrupole moments Q_t deduced from the lifetimes are shown in column 3, 4 and 5, respectively. The reduced transition probabilities were obtained by use of the expression

$$B(E2) = 8.156 \times 10^{-10} \cdot E_\gamma^{-5} \cdot \lambda(E2), \qquad (1)$$

where the reduced transition probability is in Weisskopf units (W.u.), the γ-ray energy E_γ in MeV and $\lambda = 1/\tau$

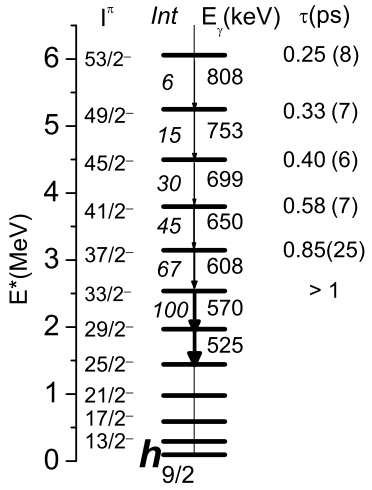

Fig. 3. The level scheme (middle column) of the $h_{9/2}$ proton 1/2[541] band in ^{171}Ta and the lifetime τ (right column) of the states extracted from their lineshapes in the present work.

Table 1. Experimental lifetimes, reduced transition probabilities and transition quadrupole moments of the proton 1/2[541] band in ^{171}Ta (W.u. = 56.379 e^2 fm^4 for $A = 171$).

I^π	E_γ (keV)	τ (ps)	$B(E2)$ (W.u.)	Q_t (eb)
$33/2^-$	570.0	> 1	< 240	< 6.23
$37/2^-$	608.5	0.85(25)	$205(^{85}_{47})$	$5.7(^{7}_{11})$
$41/2^-$	650.0	0.58(7)	$215(^{30}_{23})$	5.85(30)
$45/2^-$	699.0	0.40(6)	$217(^{38}_{28})$	5.86(44)
$49/2^-$	753.2	0.33(7)	$181(^{49}_{32})$	5.35(57)
$53/2^-$	808.5	0.25(8)	$168(^{79}_{41})$	5.14(82)

in s^{-1}. The relationship between the transition quadrupole moments (Q_t, in eb) and the lifetimes (τ, in ps) is

$$\tau = \frac{16\pi}{12.24 \times 5\langle IK20|I-2K\rangle^2} \frac{f_\gamma(E2, I \to I-2)}{E_\gamma^5(I \to I-2)Q_t^2}. \quad (2)$$

The Clebsch-Gordan coefficient can be written as

$$\langle IK20|I-2K\rangle^2 = \frac{3}{8}\frac{I(I-1)}{I^2-1/4}\left(1-K^2/I^2\right)\left(1-\frac{K^2}{(I-1)^2}\right), \quad (3)$$

where $f(E2, I \to I-2)$ is the branching ratio of the $E2$ transition which is taken to be one for the 1/2[541] band and the expression (2) can be written as

$$\tau = \frac{2.19(I^2-1/4)}{I(I-1)(1-K^2/I^2)(1-K^2/(I-1)^2)\cdot E_\gamma^5(I \to I-2)Q_t^2}. \quad (4)$$

According to the relationship [17] between the quadrupole deformation parameter β_2 and the transition quadrupole moment Q_t,

$$Q_t = \frac{3}{\sqrt{5\pi}} Z r_0^2 A^{2/3}\left(\beta_2 + \frac{2}{7}\sqrt{\frac{5}{\pi}}\beta_2^2\right). \quad (5)$$

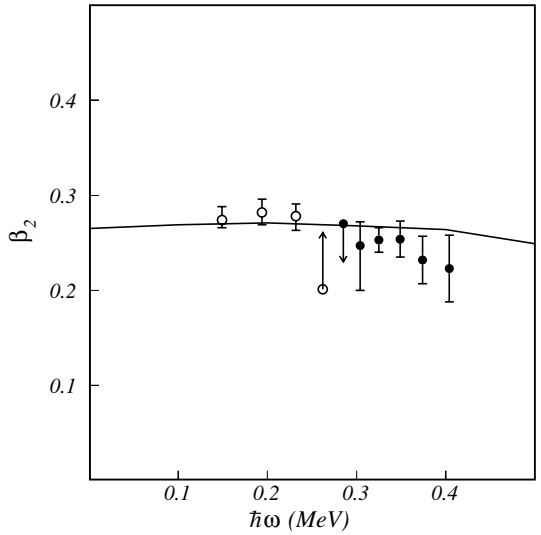

Fig. 4. Quadrupole deformation β_2 as a function of the rotational frequency ($\hbar\omega$) for the $\pi h_{9/2}1/2[541]$ band in ^{171}Ta. The full circles correspond to the results from the DSAM and the open circles to that from the RDM [18]. The solid line represents the results of TRS calculations.

The β_2 values were extracted from the data and are plotted as a function of the rotational frequency $\hbar\omega(= E_\gamma/2)$ in fig. 4. The β_2 values for the low-lying states deduced from the lifetimes measured by P. Joshi *et al.* [18] using RDM are also presented in fig. 4 for comparison. The lower and upper limits of quadrupole deformation of the 29/2 and 33/2 states are presented by arrows. It can be seen that these experimental data are smooth linked at the crossing region and they fluctuate slightly around a constant value up to $\hbar\omega \sim 0.35$ MeV, *i.e.* spin 45/2. Within the systematic errors, both data show the tendency that the β_2 and Q_t values decrease slightly with increasing rotational frequency.

Total Routhian Surface (TRS) calculations, based on the pairing deformation self-consistent cranking model, have been performed using the non-axial deformed Woods-Saxon potential [19]. In order to reduce the unphysical fluctuation of the weakened pairing field (due to the Coriolis force), an approximation of particle-number projection was used by means of the Lipkin-Nogami model [20] with pairing strengths determined by the average gap method [21]. In the pairing calculation, quadrupole pairing was included [22], which is important for rotational motion. The TRS calculated for the $h_{9/2}$ proton 1/2[541] band are shown in fig. 5 and the quadrupole deformation is 0.269, 0.271, 0.268 and 0.264 at $\hbar\omega = 0.1$, 0.2, 0.3 and 0.4 MeV, respectively. The calculated result is also shown in fig. 4 with the solid line. As can be seen, the variation of the calculated β_2 values with increasing rotational frequency is rather smooth and the nearly constant β_2 values from the theoretical calculations agree rather well with the results obtained on the basis of the lifetime measurements. The quadrupole deformation does not decrease even at the band crossing region $\hbar\omega = 0.29$ MeV, which might indicate that the structure of the three-quasiparticle band is

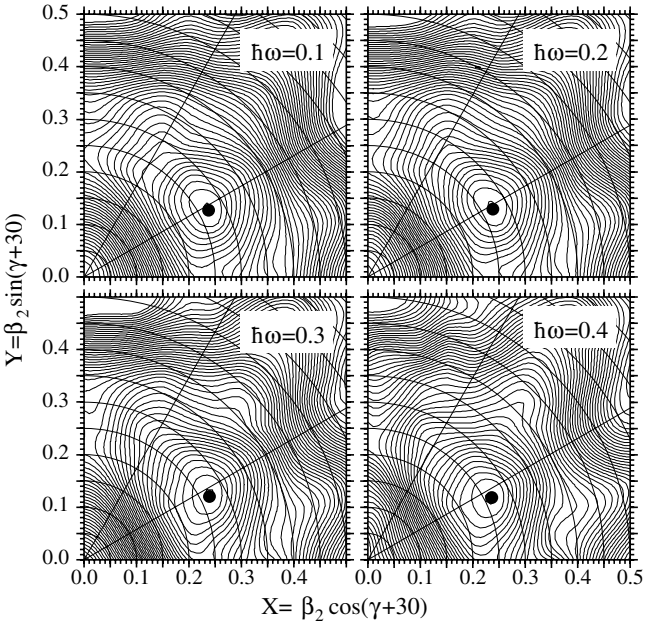

Fig. 5. The TRS plots for ^{171}Ta at frequencies of $\hbar\omega = 0.1$, 0.2, 0.3 and 0.4 MeV. Minima marked with filled circles correspond to the quadrupole deformation β_2 of 0.269, 0.271, 0.268 and 0.264, respectively.

similar to the one-quasiparticle band, or the band mixing caused by the strong interaction between these two bands is too large, which can be seen from the experimental Routhian and alignment plots [9].

The present lifetime measurement gives an average value of $\beta_2 = 0.26$ for the quadrupole deformation of the 1/2[541] band. On the other hand, R. Dogra *et al.* [23] measured the electric quadrupole moments of the $\pi h_{11/2}$ 9/2[514] band in ^{171}Ta by using the time differential perturbed angular distribution (TDPAD) method and the quadrupole deformation of $\beta_2 = 0.22$ had been extracted. This shows that the deformation is configuration dependent and the deformation of the 1/2[541] band is 18% greater than that of the 9/2[514] band, thereby demonstrating that the 1/2[541] odd proton lying at the orbital with high j and low Ω exerts a driving force on the core, favoring a more prolate shape, which might also indicate that the anomalous delay of the band crossing in the $h_{9/2}$ proton 1/2[541] band in ^{171}Ta is mainly caused by the quadrupole shape driving effect.

4 Summary

The mean lifetimes of the levels of the $\pi h_{9/2}1/2[541]$ band in ^{171}Ta were determined using the DSAM by fitting lineshapes of the γ-rays in the spectra detected at the forward and backward angles. The present measurement extends the lifetime information, which had previously been known from an RDM experiment [18], to the high-spin region of this band. The transition quadrupole moments Q_t and quadrupole deformation β_2 deduced from the measured lifetimes are not reduced at the band crossing region indicating that the one-quasiparticle band and the three-quasiparticle band are of very similar structure. In comparison with the earlier results obtained from the TDPAD method [23], the quadrupole deformation β_2 of the 1/2[541] band is 18% larger than that of the 9/2[514] band, it indicates that the anomalous delay of the band crossing of the $\pi h_{9/2}$ 1/2[541] band may mainly come from the quadrupole shape driving effect. The experimental data were also compared with theoretical results calculated within the framework of pairing-deformation self-consistent cranking shell model based on the non-axial deformed Woods-Saxon potential. The calculations show that the quadrupole deformation β_2 values keep almost constant and are in good agreement with the experimental values deduced from the lifetime measurements.

This work was supported by the National Natural Science Foundation of China under Grant Nos. 10175090, 10105015 and 10375092, and by the Major State Basic Research Development Program under Contract No. TG2000077405. We would like to thank the staff of the HI-13 tandem accelerator in the China Institute of Atomic Energy for providing a good beam condition. The authors are much indebted to Dr. G.J. Xu for preparing the targets.

References

1. C.X. Yang *et al.*, Chin. J. Nucl. Phys. **16**, 223 (1994).
2. S.J. Warburton *et al.*, Nucl. Phys. A **591**, 323 (1995).
3. H.J. Jensen *et al.*, Z. Phys. A **340**, 351 (1991).
4. H. Schnack-Petersen *et al.*, Nucl. Phys. A **594**, 175 (1995).
5. S. Ogaza *et al.*, Nucl. Phys. A **559**, 100 (1993).
6. C.H. Yu *et al.*, Nucl. Phys. A **511**, 157 (1990).
7. Theine *et al.*, Nucl. Phys. A **536**, 418 (1992).
8. S.G. Li *et al.*, Nucl. Phys. A **555**, 435 (1993).
9. J.C. Bacelar *et al.*, Nucl. Phys. A **442**, 547 (1985).
10. W. Walus *et al.*, Phys. Scr. **34**, 710 (1986).
11. H.J. Jensen *et al.*, Z. Phys. A **359**, 12 (1997).
12. R.A. Bark *et al.*, Nucl. Phys. A **644**, 29 (1999).
13. D.C. Radford, Nucl. Instrum. Methods A **361**, 297 (1995).
14. Yu.N. Lobach *et al.*, Acta Phys. Pol. B **30**, 1273 (1999), and references therein.
15. J. Lindhard, M. Scharff, H.E. Schiott, Mat.-Fys. Medd. K. Dan. Vidensk. Selsk. **33**, 14 (1963).
16. J.F. Ziegler, J.P. Biersack, V. Littmark, *The Stopping Power and Range of Ions in Solid*, Vol. **1** (Pergamon, New York, 1985).
17. W. Nazarewicz, I. Ragnarsson, *Handbook on Nuclear Properties*, edited by D.N. Poenaru, W. Greiner (Clarendon Press, Oxford, 1996).
18. P. Joshi *et al.*, Phys. Rev. C **60**, 034311 (1999).
19. W. Nazarewicz *et al.*, Nucl. Phys. A **435**, 397 (1985).
20. W. Satula, R. Wyss, P. Magierski, Nucl. Phys. A **578**, 45 (1994).
21. P. Moller, J.R. Nix, Nucl. Phys. A **536**, 20 (1992).
22. F.R. Xu, W. Satula, R. Wyss, Nucl. Phys. A **669**, 119 (2000).
23. R. Dogra *et al.*, Hyperfine Interact. **96**, 223 (1995).